Supporting Information

Combining Three Different Functional Groups in One Linker: A Variety of Features of Copper(II) Aminocarboxyphosphonate

Piotr Garczarek,[a,#] Jan K. Zaręba,[b,#,*] Marek Duczmal,[a] Jan Janczak,[c] Jerzy Zoń,[d, *] Marek Samoć,[b] and Marcin Nyk[b]

[a] Faculty of Chemistry, and [b] Advanced Materials Engineering and Modelling Group, Wrocław University of Science and Technology, Wybrzeże Wyspiańskiego 27, 50-370 Wrocław, Poland.

[c] Institute of Low Temperatures and Structure Research, Polish Academy of Sciences, 2 Okólna St., P.O.Box 1410, 50-950 Wrocław, Poland;

[d] Faculty of Mechanical and Power Engineering, Wrocław University of Science and Technology, Wybrzeże Wyspiańskiego 27, 50-370 Wrocław, Poland.

[#]those authors contributed equally

**corresponding authors: jan.zareba@pwr.edu.pl, jerzy.zon@pwr.edu.pl*

Table of contents

Asymmetric unit S2
Hydrogen bonds S2
Crystal structure projection S3
Crystallographic tables S4
TGA-DTA-MS results S5
Dehydration-rehydration experiment – IR study S7
Visible light source spectrum S9
PXRD and IR of sample after photocatalysis S9

Asymmetric unit

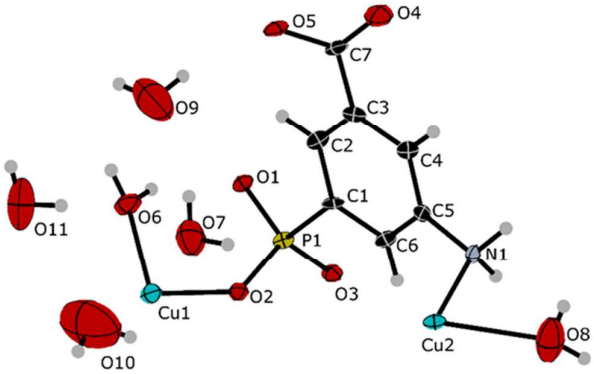

Figure S1. The asymmetric unit of 1. Displacement ellipsoids are drawn at 50% probability.

Hydrogen bonds

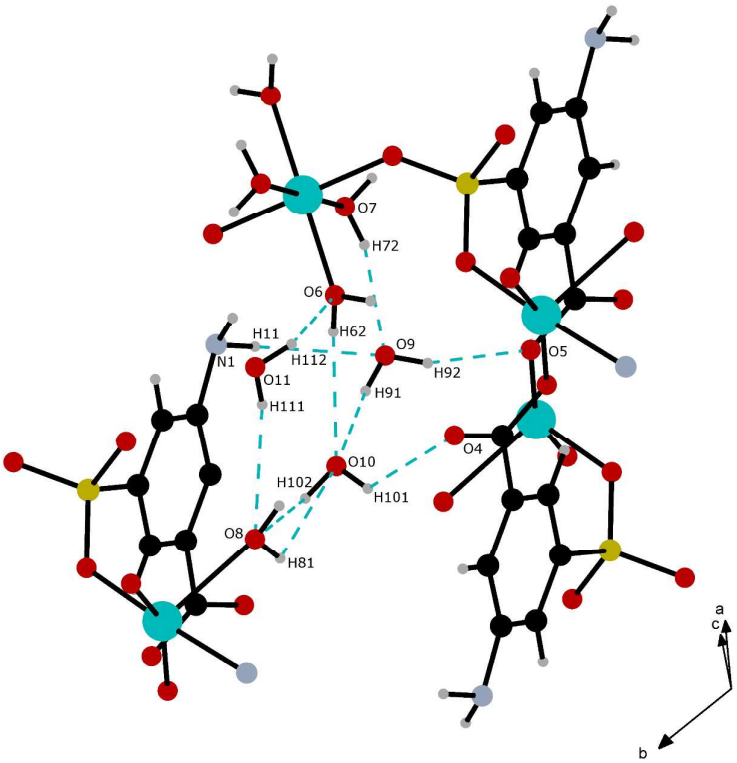

Figure S2. A projection showing hydrogen bonds present in the framework of 1.

Crystal structure projection

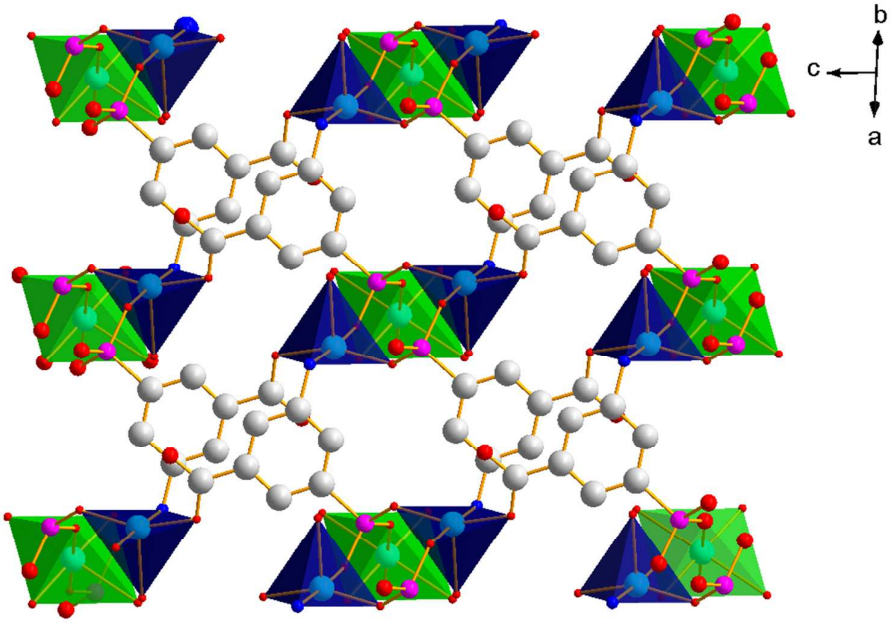

Figure S3. A projection showing inorganic and organic parts the framework of 1. Note that crystallization water has been omitted for clarity.

Crystallographic tables

Table S1. Selected bond lengths and angles (Å, °)

Bond	Length [Å]	Bond	Length [Å]
Cu1—O2	1.922(3)	Cu1—O2^{i}	1.922(3)
Cu1—O6^{i}	1.982(3)	Cu1—O6	1.982(3)
Cu2—O1^{ii}	1.947(3)	Cu2—O3^{iii}	1.949(3)
Cu2—O5^{iv}	1.960(3)	Cu2—N1	2.052(4)
Cu2—O8	2.374(4)	P1—O1	1.526(3)
P1—O2	1.515(3)	P1—O3	1.521(3)
P1—C1	1.795(4)		
Atoms	**Angle [°]**	**Atoms**	**Angle [°]**
O2—Cu1—O6^{i}	87.31(12)	O2—Cu1—O6	92.69(12)
O1^{ii}—Cu2—O3^{iii}	90.35(12)	O1^{ii}—Cu2—O5^{iv}	91.77(13)
O3^{iii}—Cu2—O5^{iv}	155.93(13)	O1^{ii}—Cu2—N1	176.41(13)
O3^{iii}—Cu2—N1	90.94(14)	O5^{iv}—Cu2—N1	88.42(14)
O1^{ii}—Cu2—O8	95.71(15)	O3^{iii}—Cu2—O8	100.28(17)
O5^{iv}—Cu2—O8	103.36(17)	N1—Cu2—O8	80.77(15)
O2—P1—O3	109.76(17)	O2—P1—O1	111.12(17)
O3—P1—O1	113.75(17)	O2—P1—C1	107.92(19)
O3—P1—C1	106.62(19)	O1—P1—C1	107.39(19)

Symmetry codes: (i) −x+1, −y+1, −z+1; (ii) x+1, y, z; (iii) −x+1, −y, −z+1; (iv) −x+1, −y, −z; (v) x−1, y, z.

Table S2. Selected hydrogen bonds.

D—H···A	D—H [Å]	H···A [Å]	D···A [Å]	D—H···A [°]
N1—H11···O9^{iii}	0.94(2)	2.54(3)	3.167(6)	124(5)
N1—H12···O2^{i}	0.92(2)	2.13(4)	2.937(5)	148(6)
O6—H61···O1	0.82(3)	1.98(4)	2.700(4)	146(5)
O6—H62···O10^{iv}	0.82(3)	2.53(3)	3.272(6)	152(6)
O7—H71···O4^{ii}	0.82(3)	2.20(2)	2.994(5)	164(7)
O7—H72···O9	0.82(3)	2.10(3)	2.885(7)	161(5)
O8—H81···O10^{i}	0.81(3)	2.60(6)	2.982(8)	111(6)
O8—H82···O7^{iii}	0.81(3)	2.38(6)	2.822(7)	115(6)
O9—H91···O10^{iv}	0.82(3)	2.43(5)	3.173(9)	151(7)
O9—H92···O5	0.82(3)	2.17(6)	2.840(6)	139(8)
O10—H101···O4^{v}	0.82(3)	2.53(5)	3.075(6)	125(6)
O10—H102···O8^{i}	0.84(3)	2.58(5)	2.982(8)	110(6)
O11—H111···O8^{vi}	0.80(3)	2.53(4)	3.228(7)	147(7)
O11—H112···O6	0.80(3)	2.15(6)	2.697(6)	126(7)
O11—H112···O11^{iv}	0.80(3)	2.42(6)	2.918(11)	122(7)

Symmetry codes: (i) −*x*+1, −*y*, −*z*+1; (ii) −*x*+1, −*y*, −*z*; (iii) *x*, *y*−1, *z*; (iv) −*x*, −*y*+1, −*z*+1; (v) *x*, *y*+1, *z*+1; (vi) *x*−1, *y*+1, *z*.

TGA-DTA-MS results

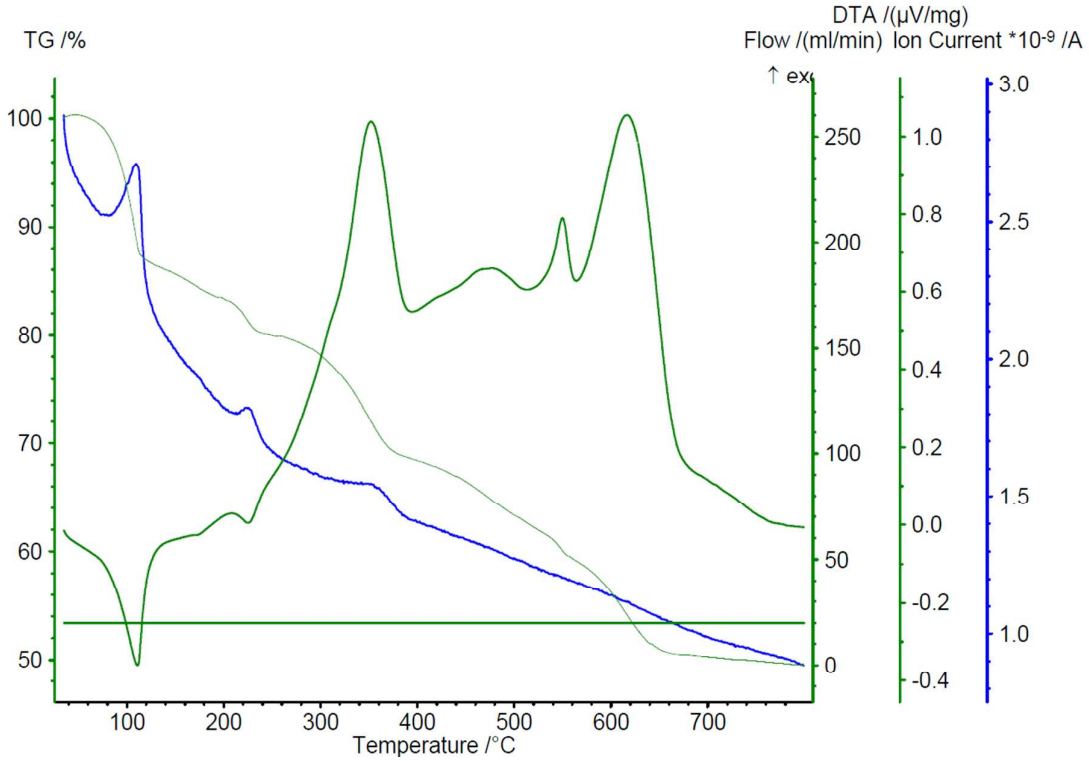

Figure S4. The MS ion current trace of H_2O (blue line) laid over TGA and DTA traces.

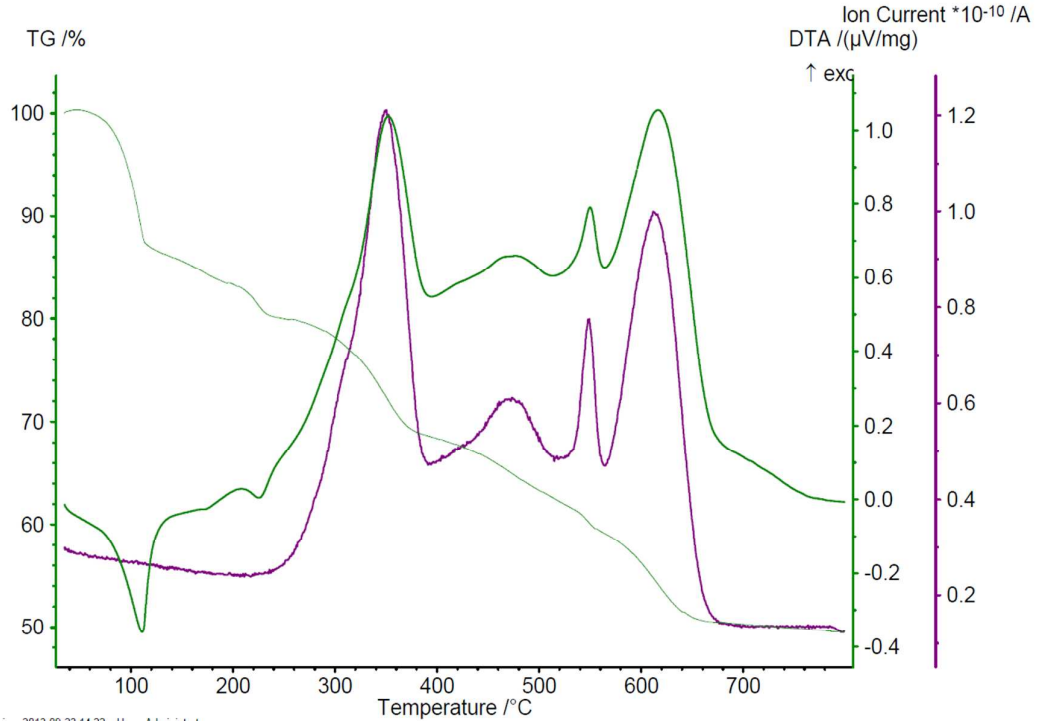

Figure S5. The MS ion current trace of CO_2 (purple line) laid over TGA and DTA traces.

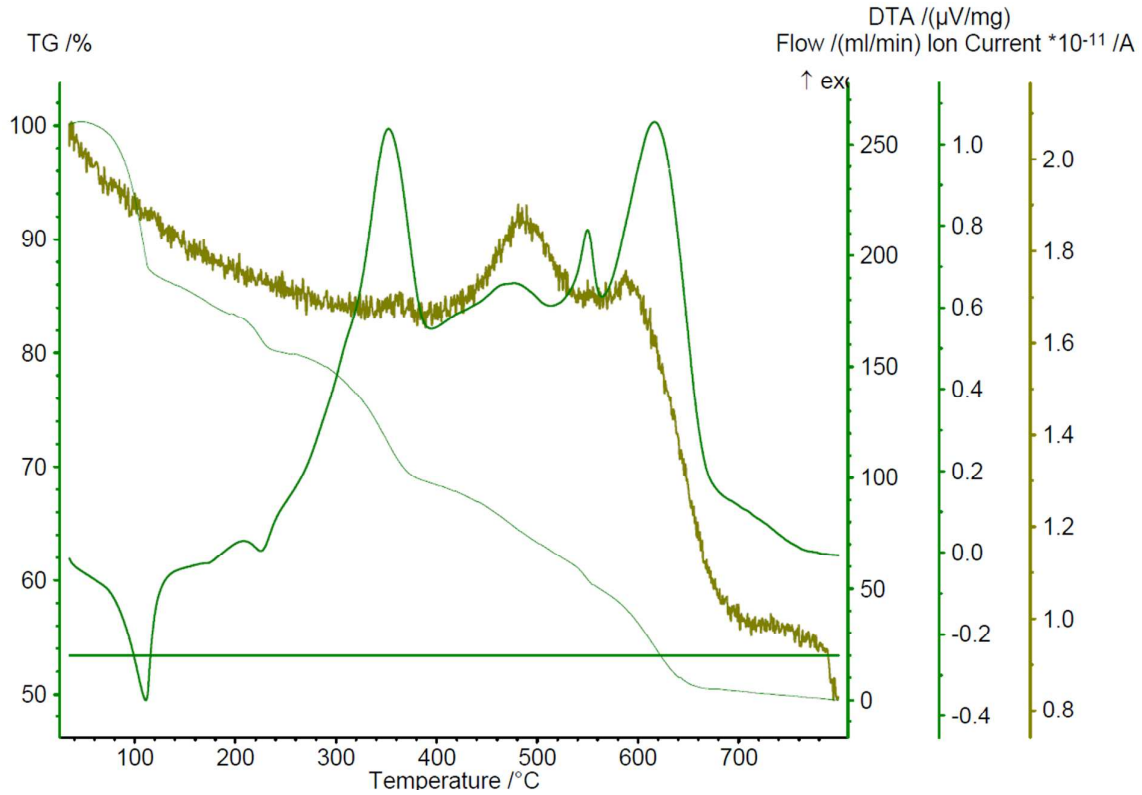

Figure S6. The MS ion current trace of NO_2 (green line) laid over TGA and DTA traces.

Dehydration-rehydration experiment – IR study

Changes both in peak intensities and positions are found in the fingerprint region (Figure S7). Upon dehydration stretching C-N vibration shifts from 1385 cm^{-1} to 1392 cm^{-1}, while stretching vibration of coordinated C-O shifts from 1553 cm^{-1} to 1545 cm^{-1}. In the 950 cm^{-1} to 1150 cm^{-1} region various O-P-O stretching modes are located, and their structure is especially complex due to low symmetry around the phosphonate group. Structural transformation leads to increase of relative intensity of component at 969 cm^{-1} as well as the splitting of the features at 1048 cm^{-1} and 1118 cm^{-1}.

In the region of IR spectrum dominated by hydrogen bonds worth emphasizing is the rise of typical sharp $–NH_2$ symmetric and asymmetric stretching feature at 3566 and 3617 cm^{-1}, respectively. In the spectrum of as-synthesized **1** this vibrational mode escapes detection, while in rehydrated samples it is noticeable after closer inspection. Although the occurring structural modification is unknown, the rise of this signal must be caused by an increase of polarity of N-H bonds, according to IR selection rules. Initially, we hypothesized that the Cu-N bond is broken during transformation, but metal coordination in fact *increases* electron demand at the nitrogen atom and its dissociation would result in decrease of intensity of that band; in light of this we suppose that the observed rise of $–NH_2$ stretching mode intensity is purely caused by removal of crystallization water (which served as hydrogen bond acceptor). Nonetheless, it should be stressed that the removal of crystallization water, participating in hydrogen-bond network, cannot be complete because broad absorption in the range 2500 – 3700 cm^{-1} in the IR spectra persists at each stage of the experiment.

Normal modes of carbon skeleton of the ligand molecule are the source of several bands, although not noticeably affected upon structural change. Most important ones are at 1608 cm^{-1}, which corresponds to stretching vibration of C=C bond, 989 cm^{-1} and 882 cm^{-1} (which

correspond to deformation vibrations of C—H bonds) and 568 cm^{-1} (which corresponds to deformation vibrations of the aromatic ring).

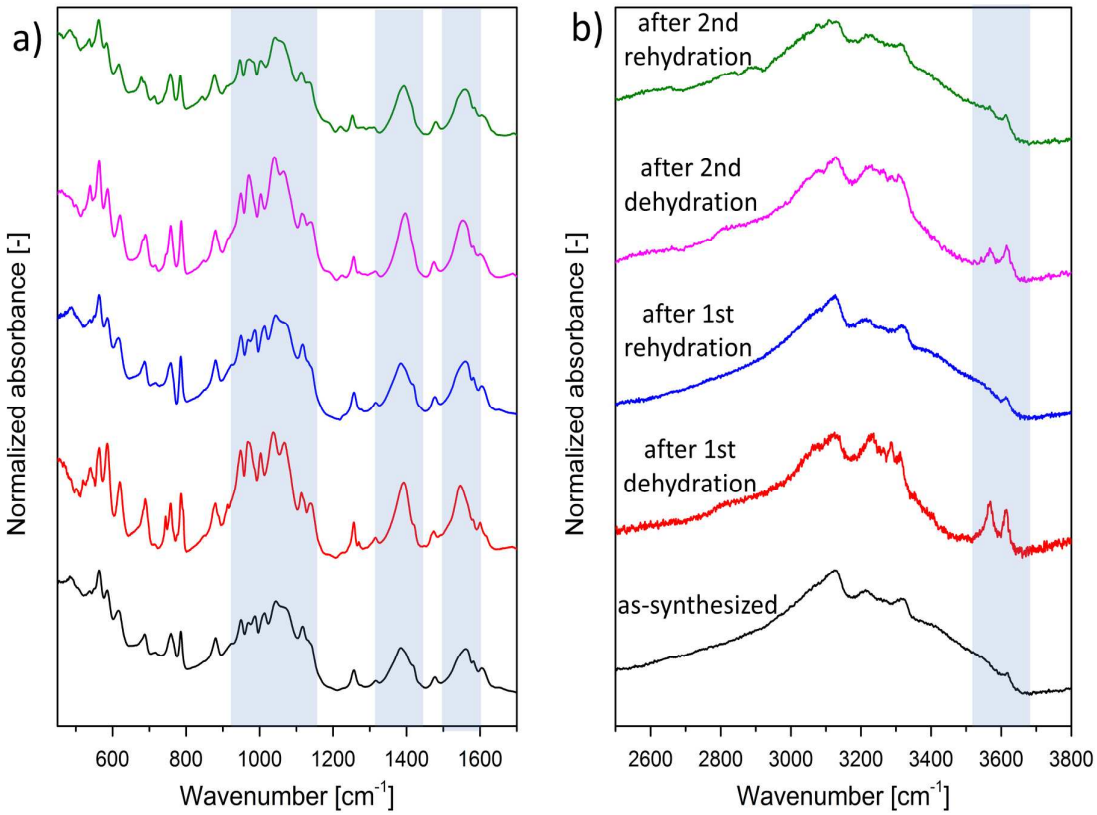

Figure S7. IR spectra of **1** in consecutive stages of dehydration-rehydration experiment. Gray areas denote regions whose shift of peak or significant change of intensity is discussed in the text.

Visible light source spectrum

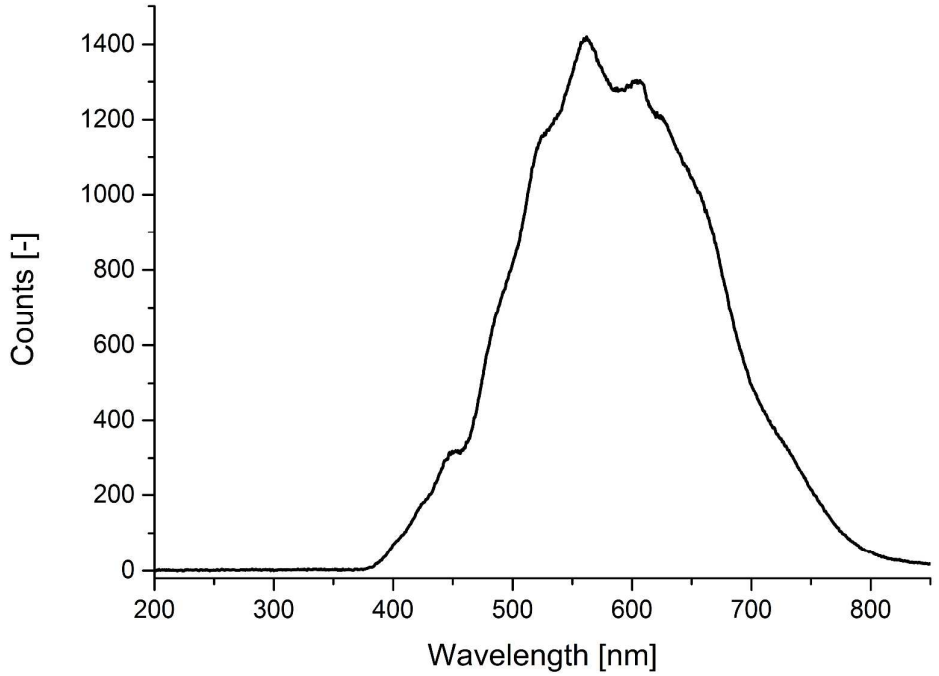

Figure S8. Emission spectrum of the used visible light source (Optel HP-250 polarized-light lamp) recorded with Ocean Optics 2000 fiber-coupled spectrograph.

PXRD and IR of sample after photocatalysis

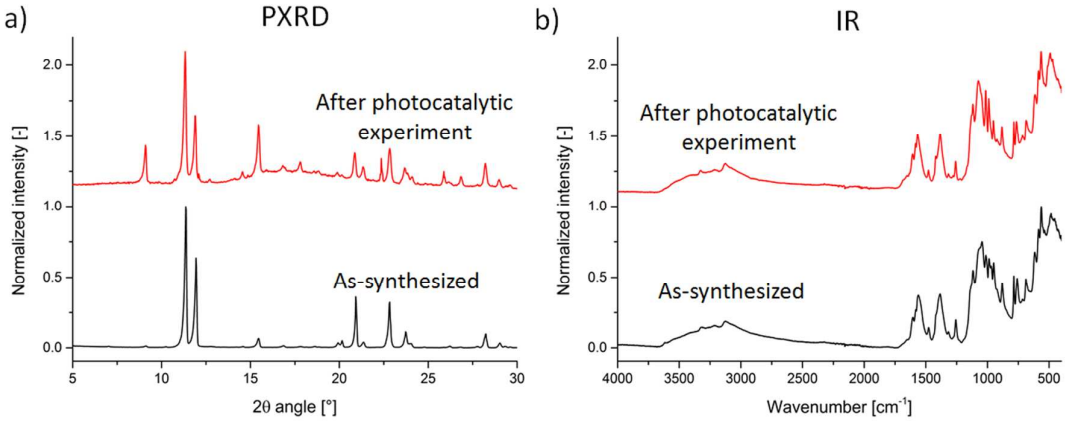

Figure S9. a) PXRD traces of compound 1 after photocatalytic experiment (upper part) and before photocatalytic experiment (lower part); b) IR spectrum of compound 1 after photocatalytic experiment (upper part) and before photocatalytic experiment (lower part)